Topographic maps of multisensory attention

Jeffrey S. Anderson[a,b,c,1], Michael A. Ferguson[c], Melissa Lopez-Larson[b,d], and Deborah Yurgelun-Todd[b,d]

[a]Division of Neuroradiology, School of Medicine, University of Utah, Salt Lake City, UT 84132; [b]The Brain Institute, University of Utah, Salt Lake City, UT 84108; [c]Department of Bioengineering, University of Utah, Salt Lake City, UT 84112; and [d]Department of Psychiatry, University of Utah, Salt Lake City, UT 84132

Edited by Marcus E. Raichle, The Washington University, St. Louis, MO, and approved October 15, 2010 (received for review August 5, 2010)

The intraparietal sulcus (IPS) region is uniquely situated at the intersection of visual, somatosensory, and auditory association cortices, ideally located for processing of multisensory attention. We examined the internal architecture of the IPS region and its connectivity to other regions in the dorsal attention and cinguloinsular networks using maximal connectivity clustering. We show with resting state fMRI data from 58 healthy adolescent and young adult volunteers that points of maximal connectivity between the IPS and other regions in the dorsal attention and cinguloinsular networks are topographically organized, with at least seven maps of the IPS region in each hemisphere. Distinct clusters of the IPS exhibited differential connectivity to auditory, visual, somatosensory, and default mode networks, suggesting local specialization within the IPS region for different sensory modalities. In an independent task activation paradigm with 16 subjects, attention to different sensory modalities showed similar functional specialization within the left intraparietal sulcus region. The default mode network, in contrast, did not show a topographical relationship between regions in the network, but rather maximal connectivity in each region to a single central cluster of the other regions. The topographical architecture of multisensory attention may represent a mechanism for specificity in top-down control of attention from dorsolateral prefrontal and lateral orbitofrontal cortex and may represent an organizational unit for multisensory representations in the brain.

attention network | fcMRI | functional connectivity | parcellation | intrinsic connectivity networks

Brain regions with related function and anatomic connectivity show synchrony of slow (<0.08 Hz) fluctuations in functional MRI (fMRI) signal (1–3). A network of brain regions known to be active during states of high attention to sensory stimuli or performance of attention-demanding tasks, the attention control network, or task positive network (4–6), reproducibly shows high functional connectivity between regions in the network. A separate interconnected network, the default mode, or task negative network (7–9), is comprised of brain regions more active during rest or attention to internal stimuli or narrative (10). We use here the nomenclature "attention control" and "default mode" networks rather than "task positive" or "task negative" networks because the positive or negative activation of each of these networks depends entirely on whether the task measures internal mentalization or attention to external stimuli (11), and both may be coactivated or have similar behavioral associations (12).

The attention control network consists of two primary subnetworks. The dorsal attention network is composed of bilateral intraparietal sulcus (IPS), frontal eye fields (FEF), and lateral prefrontal cortex (4, 5) and has also been termed the executive control network (13). This network frequently shows coactivation with the cinguloinsular, or salience detection network, consisting of bilateral anterior insula, dorsal anterior cingulate/supplementary motor area (SMA), and bilateral middle temporal (MT^+) regions (13). These networks both tend to be more active during tasks requiring higher attentional demands and may in aggregate be referred to as the attention control network (6). The attention control network may also be operationally defined as areas that are significantly correlated with IPS, MT^+, and FEF regions (6).

The IPS region is perhaps the best understood region involved in multimodal sensory attention. Lesions in the IPS region may cause neglect of modality-specific or polymodal attention (14). Auditory and visual attentional areas are processed in overlapping but distinct inferolateral and posterior subregions of the IPS (15). Distinct human IPS subregions corresponding to macaque anterior intraparietal (AIP), ventral intraparietal (VIP), medial intraparietal (MIP), lateral intraparietal (LIP), and caudal intraparietal (CIP) regions show different spatial positions within the IPS likely corresponding to functional differences in attentional modality (16). Four visual attentional areas, IPS1–IPS4 show topographic maps of human visual cortex and are situated along the posterior medial aspect of the IPS region, adjacent to area V7 (17, 18). The IPS region is thought to represent a site for top-down control of attention (4).

The default mode network consists of bilateral posterior cingulate/precuneus, medial prefrontal, temporoparietal junction, superior frontal, parahippocampal gyri, cerebellar tonsils, and inferior temporal regions (6, 8, 19) and may be defined as areas significantly correlated with posterior cingulate/precuneus, medial prefrontal, and temporparietal junction regions (6). There is converging evidence that this network participates in attending to internal stimuli or narrative and constructing a multifaceted representation of "self." Narrative-specific activation has been observed in the precuneus (20), medial prefrontal cortex (21, 22), and temporoparietal junction (22). Default mode regions show time variation with narrative stimuli (23). The default mode network has also shown greater activity during self-referential mental activity (24), including visuospatial imagery, episodic memory retrieval, and first-person perspective (10). The observation of default mode activity when subjects' minds were allowed to wander also suggests this network may process internal narrative, mentalization, and self-dialogue (25).

Both networks consist of discrete brain regions separated in space, an organization which might represent redundancy, allowing distributed processing of important brain functions, and/or specialization, where different regions perform distinct operations or compare different input streams. Clues to the functional relationship between such regions in a network can be obtained by examining the pattern of connectivity between the regions. At least three distinct patterns of connectivity are possible in such a network: there may be diffuse interconnectivity between the regions, where all voxels in a region are similarly connected to all voxels in other regions; voxels in one region may all show greatest connectivity to a central hub in other regions representing the "core" of the network; or there may be point-to-point, topographic connectivity between two or more regions. Distinguishing between such possibilities would constrain what operations could be performed on information within the network and would inform choices for targets in studying brain connectivity in neuropathology and neurodevelopment.

Author contributions: J.S.A., M.A.F., and D.Y.-T. designed research; J.S.A., M.L.-L., and D.Y.-T. performed research; J.S.A. contributed new reagents/analytic tools; J.S.A. and M.A.F. analyzed data; and J.S.A. and D.Y.-T. wrote the paper.

The authors declare no conflict of interest.

This article is a PNAS Direct Submission.

[1]To whom correspondence should be addressed. E-mail: andersonjeffs@gmail.com.

This article contains supporting information online at www.pnas.org/lookup/suppl/doi:10.1073/pnas.1011616107/-/DCSupplemental.

Results

To determine which of these models best fits the default mode and attention control networks, we applied a technique of maximal connectivity clustering to resting state fMRI time series data obtained from 58 healthy subjects. In this technique, one region in the network is selected as a test region, and correlation of time series data for each voxel in this region is calculated with each voxel in the other regions of the network. Then, the test region is divided into an arbitrary number of clusters using a *k*-means algorithm such that two test voxels will be placed in the same cluster if the voxels in each of the other regions to which the test voxels are maximally connected are sufficiently close in space. Using this technique, subdivisions of a region can be constructed that reflect the topology of its connections to the rest of a network.

For clarity, we will use the term "region" to represent a contiguous block of voxels within a network (such as left frontal eye field or right intraparietal sulcus), and "cluster" to represent a subdivision of a region. To obtain the regions in the attention control network, the mean time series from a 5-mm radius sphere in the right intraparietal sulcus (MNI coordinates $x = 50$, $y = -41$, $z = 52$) (26) was used as a seed and correlation was calculated with the time series for each voxel in the brain. Correlation values were Fisher transformed to improve normality, and a stringent threshold was used (T score > 12) for significant connectivity to the seed region across data from 58 subjects in a one-sample t-test design that identified the network as nine nonoverlapping regions: bilateral IPS, bilateral FEF, bilateral lateral prefrontal, bilateral MT^+, and SMA. An identical process was performed to identify core regions of the default mode network using a seed in the precuneus (MNI: $x = -5$, $y = -52$, $z = 40$) (26), obtaining six regions: posterior cingulate/precuneus (PCC), medial prefrontal (MPF), bilateral temporoparietal junction (TPJ), and bilateral inferior temporal (IT) cortex.

Clustering of the left intraparietal sulcus region was obtained, and the brain was partitioned by identifying with which cluster each voxel in the brain shows highest correlation. Assignments of each voxel in the attention control network to a left IPS cluster is shown in Fig. 1, for three (*Top*) and six (*Bottom*) clusters. Each voxel in each region, including the left IPS, is colored to show the left IPS cluster with which the voxel's time series is most correlated. The clustering algorithm divided this region into nearly equally sized partitions in both cases. There is homologous organization in the right IPS region, not surprising given that interhemispheric connections to homotopic brain regions are among the most robust in the brain (27) and the earliest to form (28). The lateral prefrontal region in both hemispheres separates into two topographically organized subregions, one in the more superior dorsolateral prefrontal (DLPFC) regions and one in the lateral orbitofrontal (LOF) regions, with the lateral oribitofrontal clustering inverted superior to inferior, relative to the dorsolateral prefrontal clustering. The frontal eye field, anterior cingulate, and MT^+ regions also showed topographic representations of the IPS clustering.

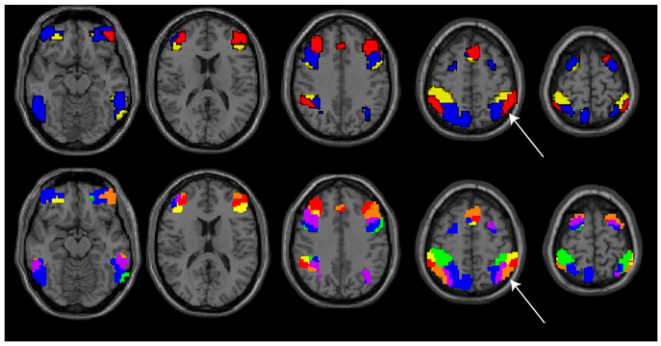

Fig. 1. Maximal connectivity clusters for the left IPS region of the attention control network. Three (*Upper*) and six (*Lower*) cluster conditions are shown. In other regions of the network, each voxel's time series is correlated with the mean time series of each left IPS cluster, and colored to correspond to the cluster with which it showed highest correlation. Slice positions are MNI: $z = -15$, 15, 35, 55, and 65. All brain images are in radiological format, with patient left on image right. The left IPS region for which the original clustering was performed is identified by arrows.

Once the clustering of the left IPS is performed, correlation can be measured between the time series of each cluster and the time series of every other voxel in the brain, including voxels outside the attention control network. Images showing which voxels in the brain have highest correlation with each cluster are presented in Fig. S1, in this case using 10 clusters in the left IPS region. MNI coordinates corresponding to highest correlation to each cluster in 13 regions of the attention control network are also tabulated in Table S1. Of these 13 regions, all 13 show geographic areas of highest correlation to at least 8 of the 10 distinct clusters (and all regions except left MT to at least 9 of the 10 clusters), organized topographically in space, with clusters that are adjacent in one region also adjacent in other regions.

It is possible that the maximal correlation patterns observed in Fig. 1 represent small differences in the mean correlation of the population but do not represent preserved topographic architecture across individual subjects. To calculate the significance of these relationships across subjects, we extracted the time series from 5-mm radius regions of interest (ROIs) surrounding coordinates of each cluster in each region listed in Table S1. Fisher-transformed Pearson correlation coefficients were measured between the time series for each of these ROIs. Each pair of regions was then considered separately, for instance right intraparietal sulcus and left MT regions. For each such pair of regions, we compared the mean correlation between the two regions for ROIs corresponding to the same clusters with the mean correlation between the two regions for ROIs corresponding to different clusters. These two measurements were obtained for each subject and each pair of regions. All 78 region pairs showed higher correlation across 58 subjects between ROIs corresponding to the same clusters than for different clusters with P value (one-tailed t test) of 0.05, corrected for multiple comparisons using the Holm-Bonferroni method (29). The P values for each region pair are shown graphically in Fig. S2.

Examining the distribution of voxels showing highest correlation to each cluster shows functionally relevant boundaries. Visual and occipital regions show highest correlation exclusively to two of the posterior medial clusters. Auditory and posterior insular cortex shows highest correlation to a single lateral cluster. Somatosensory and motor cortex show highest correlation exclusively to two of the anterior clusters. Regions of the default mode network show highest correlation to two posterior clusters.

Many of these relationships are seen in spite of the fact that other clusters may be closer to many of the voxels, strongly indicating that underlying structural connectivity relationships are responsible for the partition. The anatomical distribution of the regions of maximal connectivity to each cluster also reflect known functional specialization of the IPS; for example, the visual clusters correspond to known locations of IPS1–IPS4. Somatomotor clusters lie anteriorly, at the interface between IPS and sensorimotor cortex. The functional specialization is also analagous to the better characterized IPS subregions (AIP,VIP, MIP, CIP, and LIP) in the macaque brain. The organization of observed maximal connectivity to IPS clusters is summarized in Fig. 2.

The clustering of the IPS region corresponded closely to task activation results in an independent group of subjects. Subjects viewed images of outdoor scenes while listening to music and were instructed to focus attention on one of five conditions: visual scene, auditory features of the music, somatosensory imagery (how the scene would feel on their skin), cognitive (constructing a title for the scene), or to relax and not focus on any particular feature. The auditory, visual, and somatosensory conditions show activation with similar localization and spatial distribution to the clusters most connected to auditory, visual, or somatosensory

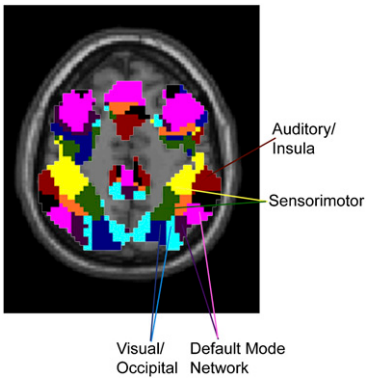

Fig. 2. Proposed functional specialization of the intraparietal sulcus region. Labels indicate brain regions that exhibited highest correlation to the specified clusters. Slice location: $z = 50$.

cortex. These results are shown in Fig. 3 for the IPS region and in Fig. S3 for the whole brain.

The clustering of the default mode network shows a different pattern from the attention control network, illustrated in Fig. 4. For this network, the posterior cingulate was selected as the test region, given evidence that this region shows the most salient interactions with other regions in the network (30). The posterior cingulate region was partitioned into relatively equal-sized clusters, but each of the other regions in the network demonstrated maximal connectivity to one central cluster in the posterior cingulate region for up to 12 cluster partitions. The size of the dominant cluster was greater than 2 SD larger than all other clusters, shown graphically in Fig. S4.

Discussion

The topographical organization of connectivity between the regions in the attention control network is reminiscent of other topographical maps in the brain, such as retinotopic, somatotopic, and tonotopic maps of the visual, somatosensory, and auditory cortex, and suggests that this network may contain multiple instances of a common information space. Given that the intraparietal sulcus is already thought to be involved in top-down control of multisensory attention (4, 17), such an information space is likely to contain a representation of polymodal attention.

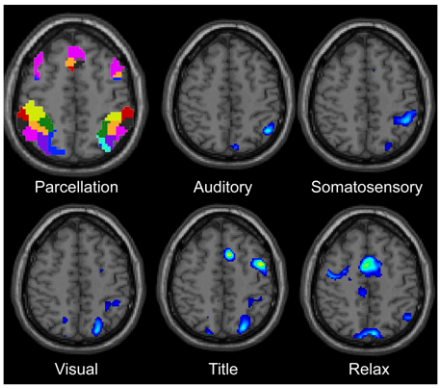

Fig. 3. Proposed functional specialization of the intraparietal sulcus region is confirmed by task activation data. All images are slice location $z = 50$. The first image shows the connectivity parcellation from the prior figure. The other five images show activation greater than 50% of peak z-scores for the five attentional conditions where subjects were instructed to focus their attention on auditory, somatosensory, visual, or cognitive (constructing a title for the scene) features of the stimuli, or to relax.

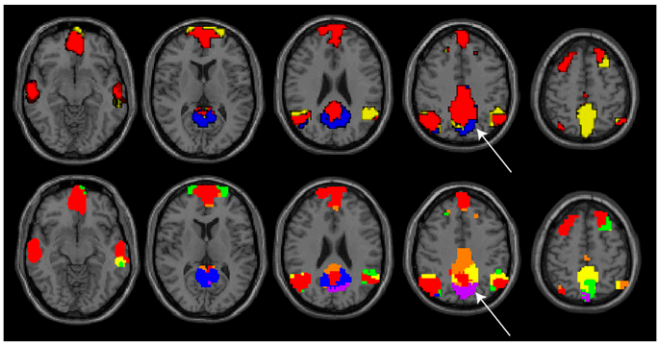

Fig. 4. Maximal connectivity clusters for the PCC region of the default mode network. Three (*Upper*) and six (*Lower*) cluster conditions are shown. In other regions of the network, each voxel's time series is correlated with the mean time series of each PCC cluster and colored to correspond to the cluster to which it showed highest correlation. The PCC region for which the original clustering was performed is identified by arrows. Slice positions are MNI: $z = -7$, 10, 25, 40, and 55.

Interactions between attention to different sensory modalities have been observed, suggesting that mechanisms for modality-specific attention are not independent. For example, a visual stimulus can enhance attention to an auditory stimulus localized to the same region of space (31). Interactions between sensory modalities can occur either due to connections between primary sensory regions or through multisensory convergence zones, and can result in competitive, additive, or superadditive effects of sensory stimulation (32). Such multisensory convergence zones pose an important problem: do attentional signals originate in these regions or do these zones act as intermediaries, receiving volitional inputs from control regions and in turn acting on sensory areas?

Current theories of attention must explain a mechanism for how top-down control architecture can generate signals in primary sensory cortex that are specific to attended areas of space and time (33). In the visual system, for example, retinotopic information is present within the intraparietal sulcus (17), and predictive models have shown how control regions such as IPS may explain numerous observed experimental results (34). Yet it is also theorized that frontal lobe regions such as frontal eye fields and prefrontal cortex may originate volitional attentional signals and act on the IPS to initiate attention (35, 36). If this is the case, then it is important that spatial and modality-specific information be present within the frontal lobe regions to effect an IPS signal that can achieve selective attention. Our results provide an organizational structure that can explain how this can occur, because topographical organization of IPS would preserve spatial and modality-selective information through connections with the frontal lobe. Moreover, we provide confirmatory task-activation data indicating subspecialization within the IPS for attention to different sensory modalities that closely corresponds to the boundaries suggested by our connectivity-based partition.

Our results also constrain the functional organization of connections between regions of the default mode network, which did not show a similar topographical organization. The default mode network thus serves as a negative control, demonstrating that the maximal connectivity clustering technique can resolve different topologies of connectivity in brain networks. Although preliminary, these results argue against a defined information space that is replicated in the multiple regions of the default mode network. Rather, our results would be more consistent with an integrative function of interoceptive and internal stimuli thought to be processed within the network. There is evidence for specialization of the regions of the default mode network into medial and temporal domains (37), which would be consistent with our results, because our technique is only sensitive for identifying patterns of connectivity between regions and not functional differences of entire regions. Similarly, a study by Margulies et al. identified three sub-

regions of the posterior cingulate/precuneus (38). Our results also showed a clustering of the posterior cingulate/precuneus roughly along a dorsal/ventral axis, but did not show topographic projections to other regions of the default mode network. This is consistent with Margulies et al., who found connectivity differences within the subregions of the posterior cingulate/precuneus primarily with areas outside of the default mode network, such as limbic, somatomotor, and dorsolateral prefrontal cortex areas (38).

Several recent reports have described methods for functional parcellations of brain regions or networks. Two primary approaches have been previously used. Seed-based approaches use several seed regions and evaluate differential connectivity to these seeds. The seeds may be chosen on the basis of architectronic atlases (39), a grid of coordinates (40), or anatomic landmarks (41). More complicated anatomy may be partitioned using the technique of Cohen et al. identifying boundaries between abrupt changes in connectivity (42). A prior parcellation of the parietal lobe using this technique has been performed (43), discriminating subregions of the left lateral parietal cortex into left IPS, anterior inferior parietal lobule, and posterior inferior parietal lobule. Our results further parcellate the left IPS into functional subdomains, with a technique most suited for evaluating within network connectivity rather than differences in connectivity to different brain regions.

It should be noted that our results do not exclude the likely possibility that other organizational schema may be present within the frontal lobes, or assess the relative importance of superimposed organizational structures. Our data do not assess for individual variations in the topographic anatomy we describe. All regions of the attention control network are significantly correlated to the other regions of the network, and the small differences in connectivity between clusters from one region to another are only evident in population data. Longer imaging times per subject or additional methods may be needed to identify individual variations in this anatomy.

With the advent of large datasets that afford the possibility of much greater statistical resolution for differences in functional connectivity (2), this technique may allow much finer discrimination of maps of attentional or other more abstract informational spaces throughout the brain. It remains unclear the extent to which individual or demographic variations in such topographical anatomy limit the ability to resolve finer anatomic detail of such maps, particularly in places such as the insula, basal ganglia, and thalamus where attentional maps, if present, may be compressed in space given the smaller size of these structures.

The topographic maps seen above also suggest an organizing principle for the frontal lobes in particular, with inverted copies of attentional space in the frontal eye field, dorsolateral prefrontal cortex, and lateral orbitofrontal cortex, and may help to define boundaries that can focus future experiments on the computations that each of these regions performs on multisensory representations. These connections may also serve to focus studies of functional connectivity in neuropathology and neurodevelopment by identifying less heterogeneous connections that may have greater functional significance in assessing connectivity disturbances or developmental changes.

Materials and Methods

Resting Subject Characteristics. Resting BOLD fMRI data were obtained from 58 normal, healthy adolescent and adult volunteers, examined after informed consent in accordance with procedures approved by the University of Utah Institutional Review Board (mean age 18.0 ± 4.9 y, age range 11–35, 32 male, 26 female.) A subset of this data has been previously reported (26). All subjects had no Diagnostic and Statistical Manual of Mental Disorders (DSM)-IV axis I diagnoses on the basis of diagnostic semistructured psychiatric interview. All participants underwent psychiatric screening via the Structured Clinical Interview for DSM-IV patient version (SCID-P), which is a widely used diagnostic instrument to reliably determine axis I disorders in clinical populations (44). All subjects were screened for anxiety by the Hamilton Anxiety Rating Scale (45) and depression by the Hamilton Depression Rating Scale (46) immediately before MRI scanning. Exclusion criteria for all subjects included: major sensorimotor handicaps; full-scale IQ <70; learning disability; history of claustrophobia, head trauma, loss of consciousness, autism, schizophrenia, anorexia or bulimia nervosa, alcohol or drug dependence/abuse based on DSM-IV criteria (during 2 mo before scan, or total past history of ≥12 mo); electroconvulsive therapy; active medical or neurological disease; metal fragments or implants; and current pregnancy or lactation. Data from two additional subjects were discarded before analysis due to excessive patient motion.

Resting Data Acquisition. Images were acquired on Siemens 3 Tesla Trio scanner with 12-channel head coil. The scanning protocol consisted of initial 1-mm isotropic MPRAGE acquisition for an anatomic template. BOLD echoplanar images (TR = 2.0 s, TE = 28 ms, GRAPPA parallel acquisition with acceleration factor = 2, 40 slices at 3-mm slice thickness, 64 × 64 matrix) were obtained during the resting state, where subjects were instructed to "Keep your eyes open and remain awake and try to let thoughts pass through your mind without focusing on any particular mental activity." Prospective motion correction was performed during BOLD imaging with PACE sequence. An 8-min resting scan (240 volumes) was obtained for each subject. An additional field map scan was obtained for each subject for the purposes of distortion correction.

For all BOLD sequences, simultaneous plethysmograph (pulse oximeter) and chest excursion (respiratory belt) waveforms were recorded for offline analysis. Waveforms were recorded directly on the scanning computer, allowing synchronization of images with physiological waveforms. Stimulus computer was synchronized to the onset of the first BOLD image via fiber optic pulse emitted by the scanner.

Attention Task Data Acquisition. For an additional 16 subjects (all different subjects from the resting state imaging sample), an attentional task was performed and BOLD images were acquired with identical imaging parameters to those above. These subjects were also normal, healthy adult volunteers imaged after informed consent (10 male, 6 female, average age 29.8 ± 8.6 y). For each subject, field map, MPRAGE, and BOLD images were obtained. The 10-min BOLD task consisted of 50 ten-second blocks of outdoor landscapes. A continuous audio soundtrack was played throughout the task with contemplative, New Age music. Before each 10-s stimulus, one of five pictorial cues were shown for 2 s: a picture of books, a couch, an ear, an eye, or a hand. Subjects were instructed to open their eyes throughout the entire task but focus their attention as directed by the cue. For books trials, they were told to construct abstract titles for the scene. For the couch trials, they were told to keep their eyes open but relax and not focus their mind on any particular feature of the stimuli. For ear trials they were told to listen to details in the music. For eye trials, they were told to pay attention to details of the visual scene. For hand trials, they were told to imagine how the scene would feel on their skin. Video monitoring during the scans confirmed that subjects' eyes were open throughout each scan.

fMRI Postprocessing. The following sequence was used for image postprocessing of all BOLD image datasets. RETROICOR (47) was performed using AFNI software package (48) for initial correction of signal components due to respiratory and cardiac artifacts. SPM8 software (Wellcome Trust) for Matlab (Mathworks) was used to perform slice timing, realign and unwarp, coregistration to MPRAGE anatomic images, segmentation of gray matter, white matter, and CSF components of MPRAGE image, normalization of MPRAGE and BOLD images to MNI template brain (T1.nii) at 3 × 3 × 3-mm resolution.

For resting state images, we additionally performed PSTCor (44) using in-house software in Matlab. Briefly, a regression analysis was performed in which the best fit of 12 time series signal components was subtracted from the time series at each voxel. Signal components were: 1, white matter time series obtained from voxels within two regions of interest in the bilateral centrum semiovale; 2, CSF time series obtained from the lateral ventricles; 3, soft tissue time series obtained from head and face; 4, respiration volume per time convolved with respiration response function (49, 50); 5, respiratory belt waveform, integrated over each TR of acquisition; 6, pulse oximeter waveform, integrated over each TR of acquisition; and 7–12, motion realignment parameters. The first 6 time series were phase shifted to optimally align with mean gray matter time series before regression. Finally, we smoothed the PSTCor-corrected BOLD images in SPM8 with full-width half-maximum kernel of 8 × 8 × 8 mm, bandpass-filtered BOLD images between 0.001 and 0.1 Hz, and performed a linear detrend at each voxel in the brain.

Identification of Default Mode and Attention Control Networks. Postprocessed time series data from each voxel of the brain in each subject were compared with time series averaged from voxels within a 5-mm radius seed in the posterior cingulate (MNI: $x = -5$, $y = -52$, $z = 40$) and right IPS (MNI: $x = 50$,

$y = -41$, $z = 52$) regions using Pearson correlation coefficients to identify the default mode and attention control networks, respectively (26). The correlation values for each subject were Fisher transformed and a second level analysis was performed in SPM8, with threshold of $T > 12$ and $T > 8$ used for high and low thresholds for significantly correlated voxels in each network. The high threshold condition resulted in four nonoverlapping regions of greater than 50 voxels in the default mode network: posterior cingulate (PCC), left temporoparietal junction (LTPJ), right temporoparietal junction (RTPJ), and medial prefrontal (MPF), and nine overlapping regions of greater than 50 voxels in the attention control network: left intraparietal sulcus (LIPS), right intraparietal sulcus (RIPS), left frontal eye field (LFEF), right frontal eye field (RFEF), left lateral prefrontal cortex (LPFC), right lateral prefrontal cortex (RPFC), supplementary motor area (SMA), left middle temporal (LMT), and right middle temporal (RMT).

Maximal Connectivity Clustering. The PCC region was chosen as a test region for the default mode network and the left IPS was chosen as a test region for the attention control network. Fisher transformed Pearson correlation coefficients were obtained for every voxel in the test region with every voxel in each of the other regions in the network. For each voxel in the test region, one voxel was selected in each of the other regions of the network that had highest correlation to the test region voxel.

For n voxels in the test region and p additional regions in the network (excluding the test region), an $n \times 3p$-size matrix was constructed. Each row corresponded to one voxel in the test region, and consisted of the x, y, and z MNI coordinates to which that voxel showed highest correlation in each of the other regions. Matrices for all of the 58 subjects were appended to form a single matrix, and a k-means clustering algorithm (kmeans.m, Matlab Statistics Toolbox) was used to evaluate the matrix 18 times, with the number of clusters used ranging from 3 to 20.

The mean time series was extracted from each of the 58 subjects and for each of the clusters in the 3, 6, and 10 cluster conditions, and correlation was computed between these time series and each voxel in the brain for each subject. An image was constructed for 3, 6, and 10 cluster conditions wherein the intensity value for each voxel in the brain was colored according to which cluster the voxel showed highest correlation to.

Attention Task Analysis. BOLD images were analyzed for each subject using block design general linear model in SPM8 to obtain whole-brain activation maps for each of the five conditions. A second level analysis in SPM8 was performed across subjects for each condition to obtain group activation maps for each of the five conditions. Whole brain images were thresholded for display at $P < 0.001$, uncorrected. For images presented in Fig. 3, a single slice through the IPS region ($z = 50$) was shown and all voxels for which group T score was 50% or higher of whole-brain peak T score were displayed.

ACKNOWLEDGMENTS. The authors thank Taylor Webb for assistance with video editing. The project described was supported by National Institutes of Health Grant RO1 DA020269 (to D.Y.-T.) and by the Ben B. and Iris M. Margolis Foundation (J.S.A.).

1. Biswal B, Yetkin FZ, Haughton VM, Hyde JS (1995) Functional connectivity in the motor cortex of resting human brain using echo-planar MRI. *Magn Reson Med* 34:537–541.
2. Biswal BB, et al. (2010) Toward discovery science of human brain function. *Proc Natl Acad Sci USA* 107:4734–4739.
3. Fox MD, Raichle ME (2007) Spontaneous fluctuations in brain activity observed with functional magnetic resonance imaging. *Nat Rev Neurosci* 8:700–711.
4. Corbetta M, Shulman GL (2002) Control of goal-directed and stimulus-driven attention in the brain. *Nat Rev Neurosci* 3:201–215.
5. Fox MD, Corbetta M, Snyder AZ, Vincent JL, Raichle ME (2006) Spontaneous neuronal activity distinguishes human dorsal and ventral attention systems. *Proc Natl Acad Sci USA* 103:10046–10051.
6. Fox MD, et al. (2005) The human brain is intrinsically organized into dynamic, anticorrelated functional networks. *Proc Natl Acad Sci USA* 102:9673–9678.
7. Uddin LQ, Clare Kelly AM, Biswal BB, Xavier Castellanos F, Milham MP (2009) Functional connectivity of default mode network components: Correlation, anticorrelation, and causality. *Hum Brain Mapp* 30:625–637.
8. Raichle ME, et al. (2001) A default mode of brain function. *Proc Natl Acad Sci USA* 98: 676–682.
9. Fair DA, et al. (2008) The maturing architecture of the brain's default network. *Proc Natl Acad Sci USA* 105:4028–4032.
10. Cavanna AE, Trimble MR (2006) The precuneus: A review of its functional anatomy and behavioural correlates. *Brain* 129:564–583.
11. Harrison BJ, et al. (2008) Consistency and functional specialization in the default mode brain network. *Proc Natl Acad Sci USA* 105:9781–9786.
12. Sadaghiani S, Hesselmann G, Kleinschmidt A (2009) Distributed and antagonistic contributions of ongoing activity fluctuations to auditory stimulus detection. *J Neurosci* 29:13410–13417.
13. Seeley WW, et al. (2007) Dissociable intrinsic connectivity networks for salience processing and executive control. *J Neurosci* 27:2349–2356.
14. Marshall JC, Fink GR (2001) Spatial cognition: Where we were and where we are. *Neuroimage* 14:S2–S7.
15. Lewis JW, Beauchamp MS, DeYoe EA (2000) A comparison of visual and auditory motion processing in human cerebral cortex. *Cereb Cortex* 10:873–888.
16. Grefkes C, Fink GR (2005) The functional organization of the intraparietal sulcus in humans and monkeys. *J Anat* 207:3–17.
17. Silver MA, Ress D, Heeger DJ (2005) Topographic maps of visual spatial attention in human parietal cortex. *J Neurophysiol* 94:1358–1371.
18. Swisher JD, Halko MA, Merabet LB, McMains SA, Somers DC (2007) Visual topography of human intraparietal sulcus. *J Neurosci* 27:5326–5337.
19. Raichle ME, Snyder AZ (2007) A default mode of brain function: A brief history of an evolving idea. *Neuroimage*, 37:1083–1090 discussion 1097–1089.
20. Whitney C, et al. (2009) Neural correlates of narrative shifts during auditory story comprehension. *Neuroimage* 47:360–366.
21. Yarkoni T, Speer NK, Zacks JM (2008) Neural substrates of narrative comprehension and memory. *Neuroimage* 41:1408–1425.
22. Troiani V, et al. (2008) Narrative speech production: An fMRI study using continuous arterial spin labeling. *Neuroimage* 40:932–939.
23. Wilson SM, Molnar-Szakacs I, Iacoboni M (2008) Beyond superior temporal cortex: Intersubject correlations in narrative speech comprehension. *Cereb Cortex* 18:230–242.
24. Gusnard DA, Akbudak E, Shulman GL, Raichle ME (2001) Medial prefrontal cortex and self-referential mental activity: Relation to a default mode of brain function. *Proc Natl Acad Sci USA* 98:4259–4264.
25. Mason MF, et al. (2007) Wandering minds: The default network and stimulus-independent thought. *Science* 315:393–395.
26. Anderson JS, et al. (2010) Network anticorrelations, global regression, and phase-shifted soft tissue correction. *Hum Brain Mapp*, 10.1002/hbm.21079.
27. Stark DE, et al. (2008) Regional variation in interhemispheric coordination of intrinsic hemodynamic fluctuations. *J Neurosci* 28:13754–13764.
28. Smyser CD, Inder TE, Shimony JS, Hill JE, Degnan AJ, et al. Longitudinal analysis of neural network development in preterm infants. *Cereb Cortex*.
29. Holm S (1979) A simple sequentially rejective multiple test procedure. *Scand J Stat* 6: 65–70.
30. Fransson P, Marrelec G (2008) The precuneus/posterior cingulate cortex plays a pivotal role in the default mode network: Evidence from a partial correlation network analysis. *Neuroimage* 42:1178–1184.
31. Busse L, Roberts KC, Crist RE, Weissman DH, Woldorff MG (2005) The spread of attention across modalities and space in a multisensory object. *Proc Natl Acad Sci USA* 102:18751–18756.
32. Driver J, Noesselt T (2008) Multisensory interplay reveals crossmodal influences on 'sensory-specific' brain regions, neural responses, and judgments. *Neuron* 57:11–23.
33. Mevorach C, Hodsoll J, Allen H, Shalev L, Humphreys G (2010) Ignoring the elephant in the room: A neural circuit to downregulate salience. *J Neurosci* 30:6072–6079.
34. Reynolds JH, Heeger DJ (2009) The normalization model of attention. *Neuron* 61: 168–185.
35. Bressler SL, Tang W, Sylvester CM, Shulman GL, Corbetta M (2008) Top-down control of human visual cortex by frontal and parietal cortex in anticipatory visual spatial attention. *J Neurosci* 28:10056–10061.
36. Monosov IE, Thompson KG (2009) Frontal eye field activity enhances object identification during covert visual search. *J Neurophysiol* 102:3656–3672.
37. Andrews-Hanna JR, Reidler JS, Sepulcre J, Poulin R, Buckner RL (2010) Functional-anatomic fractionation of the brain's default network. *Neuron* 65:550–562.
38. Margulies DS, et al. (2009) Precuneus shares intrinsic functional architecture in humans and monkeys. *Proc Natl Acad Sci USA* 106:20069–20074.
39. Roy AK, et al. (2009) Functional connectivity of the human amygdala using resting state fMRI. *Neuroimage* 45:614–626.
40. Margulies DS, et al. (2007) Mapping the functional connectivity of anterior cingulate cortex. *Neuroimage* 37:579–588.
41. Krienen FM, Buckner RL (2009) Segregated fronto-cerebellar circuits revealed by intrinsic functional connectivity. *Cereb Cortex* 19:2485–2497.
42. Cohen AL, et al. (2008) Defining functional areas in individual human brains using resting functional connectivity MRI. *Neuroimage* 41:45–57.
43. Nelson SM, et al. (2010) A parcellation scheme for human left lateral parietal cortex. *Neuron* 67:156–170.
44. First MB, Spitzer RL, Gibbon M, Williams JBW (1996) *Structured Clinical Interview for DSM-IV Axis I Disorders, Clinician Version (SCID-CV)* (American Psychiatric Press, Washington, DC).
45. Hamilton M, ed (1969) *Diagnosis and Ratings of Anxiety* (Headley, Kent, UK).
46. Hamilton M (1960) A rating scale for depression. *J Neurol Neurosurg Psychiatry* 23: 56–62.
47. Glover GH, Li TQ, Ress D (2000) Image-based method for retrospective correction of physiological motion effects in fMRI: RETROICOR. *Magn Reson Med* 44:162–167.
48. Cox RW (1996) AFNI: Software for analysis and visualization of functional magnetic resonance neuroimages. *Comput Biomed Res* 29:162–173.
49. Birn RM, Smith MA, Jones TB, Bandettini PA (2008) The respiration response function: The temporal dynamics of fMRI signal fluctuations related to changes in respiration. *Neuroimage* 40:644–654.
50. Chang C, Cunningham JP, Glover GH (2009) Influence of heart rate on the BOLD signal: The cardiac response function. *Neuroimage* 44:857–869.